

BIAN: A boundary-informed Alone Neural Network for solving PDE-constrained Inverse Problems

Kegan Li

Xi'an Jiaotong University, No.28, West Xianning Road, Xi'an, Shaanxi

E-mail: lkg818@stu.xjtu.edu.cn

November 2024

Abstract. Over the past years, inverse problems in partial differential equations have garnered increasing interest among scientists and engineers. However, due to the lack of conventional stability, nonlinearity and non-convexity, these problems are quite challenging and difficult to solve. In this work, we propose a new kind of neural network to solve the coefficient identification problems with only the boundary information. In this work, three networks has been utilized as an approximator, a generator and a discriminator, respectively. This method is particularly useful in scenarios where the coefficients of interest have a complicated structure or are difficult to represent with traditional models. Comparative analysis against traditional coefficient estimation techniques demonstrates the superiority of our approach, not only handling high-dimensional data and complex coefficient distributions adeptly by incorporating neural networks but also eliminating the necessity for extensive internal information due to the relationship between the energy distribution within the domain to the energy flux on the boundary. Several numerical examples have been presented to substantiate the merits of this algorithm including solving the Poisson equation and Helmholtz equation with spatially varying and piecewise uniform medium.

Submitted to: *Inverse Problems*

Keywords: inverse problem, neural network, collaborative neural network, convergence analysis

1. Introduction

In the field of mathematics, science, and engineering, a forward problem refers to the prediction and calculation of the behavior of a system under specific conditions based on the known system parameters or the definite conditions. Forward problems are characterized by well-defined parameters and conditions, which enable precise mathematical representations and solutions. The accurate modeling of physical problems is achievable due to their predictability and stability which in turn enables the attainment of precise solutions to forward problems through model-driven approaches. These approaches rely on the implementation of established theoretical models that encapsulate the governing laws and principles relevant to the system under study. Model-driven solutions are particularly effective when the system dynamics and the governing equations are well-defined, allowing for deterministic predictions and controlled manipulations. This approach is extensively used in fields such as physics, engineering, and economics, where reliable models form the basis for analysis, design, and optimization tasks.

In contrast to forward problems, inverse problems pertain to deduction of the causes or properties of a system from observed outcomes[1]. The lack of sufficient or unambiguous information about the physical system, accurate physical models for inverse problems presents a significant in developing. Consequently, applying model-driven methods to solve inverse problems is ineffective. Inverse problems exhibit a paucity of direct and unambiguous relationships between inputs and outputs. Consequently, alternative methodologies are imperative to address the indeterminate nature of inverse problems. Researchers have turned to data-driven technologies to confront inverse problems[2], which markedly diverge from the straightforward methodologies used in solving forward problems. The ill-posed nature of inverse problems renders the resolution of these problems with data-driven methods particularly challenging.

PDE-constrained inverse problems have wide range of applications across various fields, under scoring their significant research value. In the field of medical imaging, techniques such as computed tomography (CT), magnetic resonance imaging (MRI)[3], and ultrasound imaging rely on the solution of inverse problems to reconstruct MRI images of the interior body from external measurements. In geophysical exploration, inverse problems are employed to infer the Earth's subsurface properties from surface measurements, facilitating the search for natural resources like oil, gas, and minerals[4]. In financial market analysis, inverse problems help in modeling and predicting market behavior based on observed economic indicators[5]. Other applications include nondestructive testing, where inverse problems are utilized to identify flaws in materials and structures, and in environmental science, where they assist in understanding and predicting environmental changes based on observed data. These diverse applications demonstrate the critical role that PDE-constrained inverse problems play in advancing technology and scientific understanding.

The utilization of Scientific Machine Learning (SciML) to solve PDE-constrained inverse problems presents a number of notable advantages, over traditional numerical algorithms such as finite element methods (FEM), finite difference methods (FDM) and boundary element methods (BEM). Traditional numerical methods are primarily concerned with the resolution of well-posed boundary value problems, requiring the precise definition of boundary and initial conditions and model parameters[6]. However, the introduction of data frequently result in these methods transforming the original problem into an overdetermined system and lack the capacity to incorporate data flexibly during the solving process. This limitation renders traditional numerical methods less effective in handling of PDE-constrained inverse problems.

In contrast, SciML demonstrates considerable flexibility and effectiveness in solving inverse problems. SciML can integrate data-driven and model-driven approaches seamlessly by incorporating numerical information into objective functions, constraints, and optimization algorithms. Techniques such as deep learning and reinforcement learning enable SciML to handle large and complex datasets. Even in the absence of complete models, SciML can effectively infer system parameters or input conditions by learning patterns and relationships within the data. This hybrid approach exploits the information from both data and models, providing robust solutions to inverse problems.

Currently, research on utilizing Scientific Machine Learning (SciML) to solve inverse problems focuses on three main methods[7]:

- **Physics-Informed Neural Networks (PINNs).** The solution of inverse problems using Physics-Informed Neural Networks is achieved by embedding governing physical laws, such as partial differential equations, directly into the loss function of the neural network[8]. This integration allows the network to not only fit observed data but also maintain consistency with the underlying physical principles. By minimizing a physics-informed loss function that includes both data-fitting terms and the residuals of the governing equations, PINNs can effectively approximate unknown system parameters or inputs. This approach combines the strengths of data-driven methods with the rigor of model-driven approaches, ensuring that the inferred solution adheres to the physical behavior of the system. Additionally, the physics-based regularization introduced by PINNs enhances the robustness and accuracy of the solution, even in scenarios with incomplete, sparse, or noisy data. This makes PINNs a powerful tool for solving both forward and inverse problems in complex physical systems.
- **Deep Ritz Method (DRM).** The Deep Ritz Method (DRM) offers a variational approach to solving inverse problems by utilizing the principles of the Ritz method, where the solution of a PDE is obtained by minimizing an associated energy functional[9]. In DRM, a neural network is trained to approximate the solution by minimizing the energy functional that corresponds to the underlying PDE. This method efficiently captures the physical phenomena described by the PDE while leveraging the expressive capacity of neural networks to handle complex,

high-dimensional data. By integrating neural networks with variational principles, DRM provides a robust framework for solving inverse problems, particularly those characterized by complex geometries and boundary conditions. The method is highly versatile, capable of approximating solutions with high accuracy even in situations where traditional numerical methods may struggle due to the problem's dimensionality or the presence of noise in the data.

- **Weak Adversarial Networks (WANs).** Weak Adversarial Networks (WANs) address inverse problems by employing the weak formulation of PDEs and integrating adversarial learning into the neural network training process[10]. In this approach, the neural network is trained to approximate the solution of the PDE by minimizing a loss function that incorporates the weak form of the PDE, while an adversarial network is employed to improve the solution's precision. The adversarial network iteratively refines the candidate solution by distinguishing between accurate and less accurate approximations, guiding the primary network toward a more physically consistent solution. This approach enables WANs to effectively learn the underlying physical laws from observational data, even in the presence of noise and incomplete information. The adversarial component enhances the network's capacity to handle challenging problems, providing a flexible and robust framework for solving complex inverse problems in scientific and engineering applications.

Nevertheless, the physical governing equation employed by these inverse problems-solving methods are defined within the solution domain. This necessitates the measurement data from internal domain for the inverse prediction of unknown model parameters and the forward computation of unknown physical field quantities. Consequently, invasive measurements are particularly challenge, especially for certain entities. Moreover, the volume of required measurement data increase exponentially with the dimensionality of the solution domain. This limitations restrict the effectiveness and applicability of SciML in addressing PDE-constrained inverse problems.

To further enhance the applicability of SciML in solving inverse problems, we propose a novel neural network model that relies exclusively on the boundary data of the solution domain: Boundary-Informed Alone Neural Network (BIAN). The advancement of the proposed deep learning-based approach is derived from the so-called equivalence principle which involves transforming the absent physical information in the governing equations into unknown equivalent excitation sources and establishing an equivalent transformed relationship between the energy distribution in the solution domain and the energy flux at the boundaries by using the Green's theorem[11]. This method employs boundary forward information to inversely predict the distribution of the equivalent excitation sources, thereby determining the unknown physical information and field distributions. In summary, the BIAN not only simplifies the data acquisition but also reduces the volume of the requirement measurements, thus increasing its utility for practical physics and engineering applications.

To improve the accuracy and robustness of this algorithm, we propose a collaborative optimization model consisting of multi-neural networks. This model incorporates three types of neural networks: a fully connected neural network (FCNN) as serving an approximator, another fully connected neural network as a generator, and a single-layer neural network acting as the discriminator. The FCNN approximator is responsible for absent estimating the missing physical information in the governing equations, the generator predicts the solution, and the discriminator evaluates the accuracy of the samples generated by the generator on the boundaries and domains. Since the predictions from the approximator and the generator can be represented in a closed form, the information exchange is permitted during the training process of these multiple neural networks. This results in a collaborative relationship between the networks rather than an adversarial one typical of generative adversarial networks. This enhances the prediction accuracy, convergence efficiency and stability of the multi-neural network model.

An overview of this paper is as follows. Section 2 is dedicated to our proposed approach for learning a neural network for the indeterminate coefficients. We describe topics including the mathematical framework, the structure of the network and the optimization methodology. The convergence analysis of BIAN has been established in Section 3. In Section 4, we focus on the numerical examples that illustrate the benefits and potential of our approach in inverse problems with complex medium distributions. Finally, the conclusion and future work are provided in Section 5.

2. The Algorithm

This section examines the theoretical foundation of Boundary-Informed Alone Neural Network. The exploration encompasses three main components: the mathematical model of PDE-constrained inverse problems, the mathematical solution of BIAN, and the multiple neural network system utilized in this method.

2.1. Mathematical Model of PDE-constrained inverse problems

Firstly, we present the mathematical model for the PDE-constrained inverse problems. These problems involve the determination of unknown parameters in a system based on given responses or observed data. Mathematically, these problems can be expressed as follows:

$$\mathcal{F}(u, \varepsilon) = f \tag{2.1}$$

where \mathcal{F} is the operator that describes the behavior of the system. u represents a state variable of the system, such as temperature, displacement, or electric potential, while ε denotes a parameter to be identified, such as material properties or source terms. The term f represents a known response or output of the system. The objective of parameter identification is to determine the optional estimate $\hat{\varepsilon}$ that minimizes the discrepancy between $\mathcal{F}(u, \hat{\varepsilon})$ and f .

However, we may encounter several challenges when solving such PDE-constrained inverse problems[12]:

- **Ill-posedness.** One of the primary challenges in PDE-constrained inverse problems is their ill-posed nature. According to Hadamard’s definition, a problem is well-posed if it has a unique solution that depends continuously on the input data. In contrast, an ill-posed problem may fail to meet one or more of these criteria. For instance, an ill-posed problem may be no solution, multiple solutions, or solutions that are highly sensitive to minor perturbations in the input data. This sensitivity to measurement noise and errors can result in significant inaccuracies in the identified parameters, making it difficult to obtain reliable and stable solutions.
- **Nonlinearity.** Another challenge is the inherent nonlinearity in the relationship among the state variable u , the parameter ε , and the system response f . In many physical and engineering systems, the governing equations are represented by nonlinear differential equations. This nonlinearity complicates the identification process as the solution space is not straightforward and may contain multiple local minima. To navigate this complex landscape nonlinear optimization techniques are necessary, although these can be computationally intensive and require sophisticated algorithms to ensure convergence to the global optimum.
- **High Dimensionality.** Parameter identification problems can also involve numerous parameters, thus giving rise to high-dimensional optimization problems. High dimensionality significantly increases the complexity of the problem. The computational cost grows exponentially with the number of parameters, a phenomenon known as the "curse of dimensionality." Moreover, high-dimensional spaces may be sparsely populated with data points, complicating the construction of accurate models and increasing the risk of overfitting. Efficient algorithms and dimensionality reduction techniques is essential to manage this complexity and make the optimization problem tractable.

2.2. Mathematical Solution of BIAN

BIAN is proposed to leverage boundary information to accurately predict the internal distribution of unknown excitation source, medium parameters and field quantities, using only boundary information. The mathematical solution seeks to transform the governing equations of the system into a form that can be solved using boundary data alone.

This is a claim by establishing a relationship between the energy distribution within the domain and the energy flux of the boundaries, thereby eliminating the necessity for internal information required to solve PDEs. To illustrate a two-dimensional potential problem with an unknown medium distribution, consider its mathematical model is as follows,

$$\mathcal{L}(u(x), \varepsilon(x)) = f(x), \quad x \in \Omega \quad (2.2a)$$

$$u(x) = p(x), \quad x \in \Gamma_1 \quad (2.2b)$$

$$\frac{\partial u(x)}{\partial \mathbf{n}} = q(x), \quad x \in \Gamma_2 \quad (2.2c)$$

where \mathcal{L} is the differential operator, i.e. $\mathcal{L}(u(x), \varepsilon(x)) = -\nabla \cdot (\varepsilon(x)\nabla u(x))$, $\varepsilon(x)$ represents the indeterminate medium distribution. $f(x)$ is the source term and $\Gamma_1 + \Gamma_2 = \partial\Omega$ is the boundary of the solution domain Ω . $p(x)$ and $q(x)$ denote the essential boundary condition and the natural boundary condition for the potential problem.

The first step of this method involves transforming the medium into equivalent excitation source. The equivalent source derived using the vector equation $-\nabla \cdot (\varepsilon\nabla u) = -\varepsilon\nabla \cdot \nabla u - \nabla\varepsilon \cdot \nabla u$ and the governing equation is expressed as

$$-\nabla^2 u(x) = g(x) \quad (2.3)$$

where $g(x) = (f(x) + \nabla\varepsilon(x)\nabla u(x))/\varepsilon(x)$ donates the equivalent source term. Consequently, original potential problem has been reformulated to include an unknown excitation source term.

The Green's function, $G(x, x')$, is defined as the response of a system at a point x due to a unit impulse source applied at another point x' . Mathematically, the Green's function satisfies the following fundamental equation, where $\delta(x - x')$ is the Dirac delta function

$$\nabla^2 G(x, x') + \delta(x - x') = 0 \quad (2.4)$$

The objective of the following section is to establish the relationship between the energy distribution within the solution domain and the energy flux at the boundary. To this end, we propose the weighted residual approach that utilizes the Green's function as the weight function. The weight residual function is expressed as:

$$\int_{\Omega} G \cdot (\nabla^2 u + g) d\Omega = 0 \quad (2.5)$$

By using integration by parts, we can rewrite Equation (2.5) as

$$\begin{aligned} \int_{\Omega} G(\nabla^2 u + g) d\Omega = \\ \int_{\Omega} \nabla(G\nabla u) d\Omega - \int_{\Omega} \nabla u \cdot \nabla G d\Omega + \int_{\Omega} Gg d\Omega \end{aligned} \quad (2.6)$$

A second application of integration by parts to the second integral term on the right-hand-side of Equation (2.5), yields

$$\begin{aligned} \int_{\Omega} \nabla u \cdot \nabla G d\Omega = \\ \int_{\Omega} \nabla(u\nabla G) d\Omega - \int_{\Omega} u\nabla^2 G d\Omega \end{aligned} \quad (2.7)$$

The Gauss's theorem, with the form of Equation (2.7), can be employed to derive an equation that has been applied to establish relates the energy distribution within the domain to the energy flux at the boundaries.

$$\int_{\Omega} (\nabla F) d\Omega = \oint_{\partial\Omega} F \cdot d\vec{S} \quad (2.8)$$

The relationship between these two kinds of energy can be established as:

$$c(x'_b)u(x'_b) = \int_{\Gamma} (G(x_b, x'_b)\nabla u(x_b) - u(x_b)\nabla G(x_b, x'_b)) \cdot d\Gamma + \int_{\Omega} G(x_i, x'_b)g(x_i)d\Omega \quad (2.9)$$

The value of $c(x'_b)$ is dependent upon the location of the source point x'_b . Specifically, $c(x'_b) = 1 - a/2\pi$ when the source point x'_b is situated on the boundary of the domain, where a is the angle constituted by the tangent plane at the boundary point x'_b . x_b and x_i are the boundary and interior field points, respectively.

When the source point x'_i is located within the domain Ω , the properties of the Dirac delta function dictate that $c(x'_i)$ is equal to 1, we can get the relationship between the internal points and the boundary condition with the form:

$$u(x'_i) = \int_{\Gamma} (G(x_b, x'_i)\nabla u(x_b) - u(x_b)\nabla G(x_b, x'_i)) \cdot d\Gamma + \int_{\Omega} G(x_i, x'_i)g(x_i)d\Omega \quad (2.10)$$

Through the above method, we represent the energy distribution within the solution domain using the boundary energy flux, resulting in an energy equation that relies solely on boundary information. Next, we introduce how to use neural networks to approximate the medium parameters and potential distributions.

2.3. The Multiple Neural Network System

The aforementioned method yields an energy conservation equation from boundary information to characterize the distribution of unknown equivalent excitation sources within the solution domain. We will subsequently explain how neural network system can be used to predict the unknown medium parameters and potential distributions.

The fundamental premise of multi-neural network is to leverage the strengths of various networks to address the limitations inherent in a single neural network. The networks may be configured with different topologic parameters, and training methodologies tailored to suit varying tasks and data characteristics.

The integration of various network enables multi-neural networks to capture the intricate characteristics of data in a more comprehensive manner, thereby improving the accuracy of predictions. However, the computational cost of training multi-neural networks is typically higher than that of training a single neural network. A notable example is the generative adversarial network (GAN)[13], which consists of two neural networks, a generator and a discriminator, engaging in an adversarial game to ultimately identify the Nash equilibrium point. Consequently, a prevalent challenge associated with GAN is the instability of the training process.

In this paper, we propose a multi-neural network system incorporating an approximator, a generator and a discriminator. The approximator estimates the indeterminate medium distribution, the generator generates the solution function of the PDE, and the discriminator assessed the accuracy of the generated solution. Given the optional solutions for the generator and approximator networks can be expressed in closed form with respect to each other, it follows that the relationship between these two networks should be collaborative rather than competitive. Therefore, this paper will focus on the collaborative training methodology that shares intermediate computational results between the generator and approximator, with the aim of improving training efficiency and model performance.

2.3.1. The approximator The approximator serves to approximate the indeterminate medium distributions in the physical equation. The employed network architecture consists of input and output layers along with two residual blocks, each comprising two linear transformations, two activation functions and a residual connection. The input $x_{(i-1)}$ and the output x_i of the residual block are both m -dimensional vectors. The residual block of the neural network can be mathematical represented as

$$x_i = f_{\vartheta}^{i-1}(x_{i-1}; \vartheta) = \sigma(W_{i-1}^2 \cdot \sigma(W_{i-1}^1 x_{i-1} + b_{i-1}^1) + b_{i-1}^2) + x_{i-1} \quad (2.11)$$

where $W_{(i-1)}^1, W_{(i-1)}^2 \in R^{(m \times m)}$, $b_{(i-1)}^1, b_{(i-1)}^2 \in R^m$ are the parameters of the residual block and $\sigma(x)$ donates the activation function. To avoid the gradient vanishing issue caused by the sigmoid function and the neuron death problem caused by the ReLU function, we choose the Swish function[14] as the activation function in the following form:

$$\sigma(x) = x \cdot \text{sigmoid}(x) = \frac{x}{1 + e^{-x}} \quad (2.12)$$

The last term of Equation (2.11), the residual connection, is a mature architecture in deep learning to enhance the performance of the model. The importation of the residual connection helps to address the vanishing gradient problem and the degradation problem[15]. Figure 1 illustrates the structure of the residual block neural network, which can be mathematically represented as:

$$u_1(x; \theta) = W_{output} \cdot (f_{\vartheta}^2 \circ f_{\vartheta}^1(\sigma(W_{input} \cdot x + b_{input}))) + b_{output} \quad (2.13)$$

where θ donates the full parameters of the neural network, including the weight and bias in the residual blocks and the input and output layers. The symbol \circ represents function composition, which means applying functions in sequence.

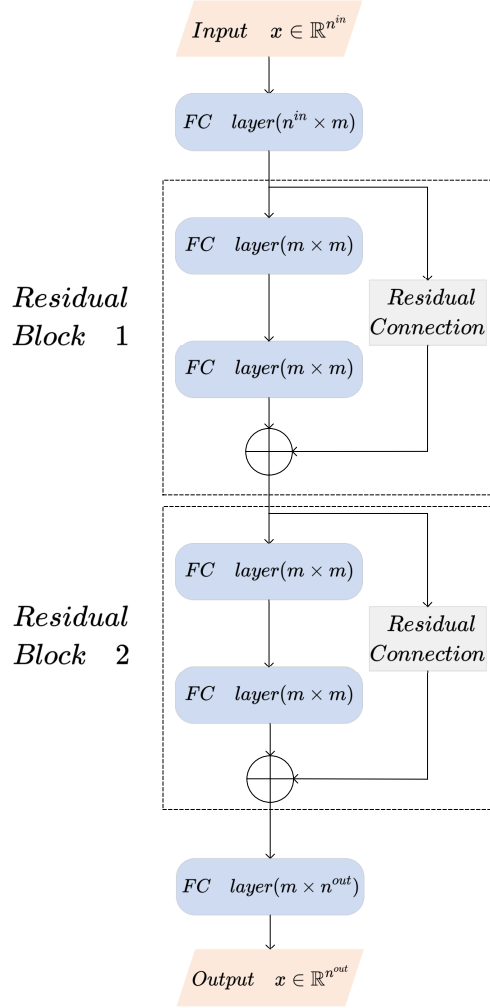


Figure 1. The structure of the neural network used in this work. Two residual blocks and two extra fully connected layers are employed.

Employing the approximator neural network u_a instead of the source term $g(x)$ in Equation (2.9) enables the definition of the residual function, which guides the training of the neural network to facilitate the learning of the indeterminate medium distribution, the residual at a given boundary source point x'_b can be expressed as follows.

$$\begin{aligned}
 R_a(x'_b; \theta_a) &= c(x'_b)u(x'_b) + \int_{\Gamma} u(x_b)\nabla G(x_b, x'_b) \cdot d\mathbf{\Gamma}(x_b) \\
 &\quad - \int_{\Gamma} G(x_b, x'_b)\nabla u(x_b) \cdot d\mathbf{\Gamma}(x_b) - \int_{\Omega} G(x_i, x'_b)u_a(x_i; \theta_a)d\Omega(x_i) \quad (2.14)
 \end{aligned}$$

Specifically, assuming m_b source points x'_b are allocated on the boundary the loss function is then considered to be the average of the sum of the squares of the residuals among the source points $\{x'_b\}$. This can be expressed as follows,

$$Loss_a(x'_b; \theta_a) = \frac{1}{m_b} \sum_{i=1}^{m_b} ||R_a(x'_b; \theta_a)||^2 \quad (2.15)$$

The equivalent source term can be obtained by minimizing the loss function through the training process:

$$\theta_a^* = \arg \min_{\theta \in \Theta_a} Loss_a(x'_b; \theta_a) \quad (2.16)$$

2.3.2. The Generator However, employing a single neural network does not directly yield the solution function for the coefficient identification problems we aim to solve. To address this, we introduce a second neural network as a generator. Similar to the approximator, we utilize a neural network with two residual blocks, which has the same form as the approximator.

The generator employs the same neural network architecture as the approximator, specifically a network comprising two residual blocks. By substituting the generator network u_g at the internal source points x'_i in Equation (2.10), we define the residual function, which guides the training of the neural network to learn the solution function. The residual at a given internal source point x'_i can be expressed as

$$\begin{aligned} R_g(x'_i; \theta_g) &= u_g(x'_i) + \int_{\Gamma} u(x_b) \nabla G(x_b, x'_i) \cdot d\Gamma(\mathbf{x}_b) \\ &- \int_{\Gamma} G(x_b, x'_i) \nabla u(x_b) \cdot d\Gamma(\mathbf{x}_b) - \int_{\Omega} G(x_i, x'_i) u_a(x_i; \theta_a) d\Omega(x_i) \end{aligned} \quad (2.17)$$

specifically, assuming m_i source points x'_i are distributed inside the domain, the loss function is defined as the average of the sum of the squares of the residuals among the source points $\{x'_{i_j}\}$. This can be expressed as follows,

$$Loss_g(x'_{i_j}; \theta_g) = \frac{1}{m_i} \sum_{j=1}^{m_i} \|R_a(x'_{i_j}; \theta_g)\|^2 \quad (2.18)$$

The equivalent source term can be obtained by minimizing the loss function through the training process:

$$\theta_g^* = \arg \min_{\theta \in \Theta_g} Loss_g(x'_i; \theta_g) \quad (2.19)$$

Training the approximator $u_a(x)$ and the generator $u_g(x)$ enables the derivations of the equivalent source term $g(x)$ and the solution function $u(x)$. The derived equivalent source and solution can subsequently be used to infer the indeterminate medium distributions. The relationship between the indeterminate medium parameters and the given source is expressed as,

$$g(x) = (f(x) + \nabla \varepsilon(x) \nabla u(x)) / \varepsilon(x) \quad (2.20)$$

This collaborative approach between the two neural networks ensures the accuracy and validity of the solution to the inverse problem, which also satisfying the relevant physical constraints and boundary conditions.

2.3.3. The Discriminator To enhance the accuracy and consistency of predictions from the approximator and generator networks in a hybrid physics-data-driven model,

we introduce a single-layer neural network as a discriminator. This discriminator assesses the accuracy of generated solutions by comparing them with known boundary conditions, thus helping to refine predictions from the approximator and generator networks for higher accuracy and consistency.

When solving PDE-constrained inverse problems using numerical algorithm, it is often assumed that increasing the number of interior source points could lead to higher accuracy in the solution. However, this approach does not necessarily yield better results when using BIAN. The accuracy of solutions obtained through BIAN is primarily influenced by the precision of the boundary discretization and the treatment of boundary conditions, especially at the corner points. Simply adding more interior source points may increase computational complexity without improving the accuracy of the solution. Therefore, it is preferable to reduce the error of BIAN by increasing the boundary source points.

Through averaging the errors among the boundary points, the overall error solving with the boundary integral equation can be reduced[16]. Therefore, the discriminator assesses the error distribution by calculating the JS divergence, a non-symmetric measure of the difference between two probability distributions[17] with the form as Equation (2.21), between the error distribution of the result of generator at boundary points and the given boundary conditions versus a uniform error distribution.

$$M(x) = \frac{1}{2}(P(x) + Q(x))$$

$$D_{JS}(P||Q) = \int_{-\infty}^{\infty} P(x)\log_2\frac{P(x)}{M(x)} + Q(x)\log_2\frac{Q(x)}{M(x)}dx \quad (2.21)$$

The JS divergence indicates the extent to which distribution $Q(x)$ deviates from distribution $P(x)$. If $P(x) = Q(x)$, the result of JS divergence equals 0. And the maximum of JS divergence equals 1 in the case where two probability distributions $P(x)$ and $Q(x)$ do not overlap at all.

By considering the output of the discriminator, $D(x)$, if this output exceeds a certain value, in this algorithm the threshold value is set to 0.1, we will double the number of source points at the corner points on the boundary. Then we retrain the neural network until the output of the discriminator is less than the set threshold value.

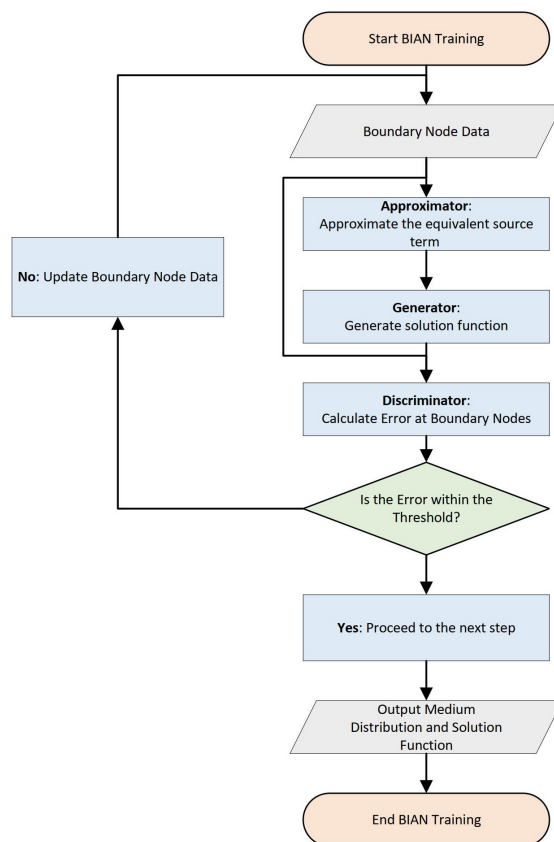


Figure 2. The algorithm flow of BIAN.

This section introduces a novel multi-neural network collaborative optimization model. The integration of approximator, generator and discriminator in the collaborative training process effectively addressed challenges inherent in inverse problems, such as ill-posedness, nonlinearity and high dimensionality. The BIAN algorithm provides a robust framework for accurately identifying unknown parameters in PDEs and serves as a powerful tool for solving a wide range of physical and engineering problems. In conclusion, we present the BIAN algorithm flow as summarized in Algorithm 1 and the flowchart is shown as Figure 2.

Algorithm 1 Algorithm of BIAN

Input: Distributed boundary and interior field points x_b, x_i and source points x'_b, x'_i .**Output:** Distribution of the solution function and internal medium distribution.

- 1: Calculate the Green function for each boundary and interior source point with respect to boundary and interior field points.
 - 2: Initialize the parameters of the approximator, generator, and discriminator networks, and set the training step size, number of iterations, and the JS divergence threshold value a .
 - 3: **for** $i = 1, 2, \dots, N$ **do**
 - 4: **if** $D(x) \leq a$ **then**
 - 5: **break**
 - 6: **else**
 - 7: Calculate an initial approximation of the equivalent source term using the approximator network.
 - 8: Utilize the approximation results from the approximator to obtain an initial generated output of solution function using the generator network.
 - 9: Pass the output of generator to the discriminator, which calculates the JS divergence between the error distribution of the result of generator at boundary points and the given boundary conditions versus a uniform error distribution.
 - 10: Refine the first two networks utilizing the feedback from the discriminator network.
 - 11: **end if**
 - 12: **end for**
 - 13: After the training process, both the medium distributions and the solution function are solved.
-

3. The Convergence Analysis of BIAN

Many efforts have been devoted to the development of the convergence theory for the SciML to solve PDE-constrained inverse problems. In [18], the authors discuss the convergence and generalization issues of PINN and analyze the performance of PINN on various problems and provide derivations of the error bounds. [19, 20] study the convergence rate of DRM with two layer networks and deep networks. The convergence of WAN has been proved in [21]. In this section, we provide a rigorous convergence theory for BIAN with respect to the amount of training data. By employing probabilistic space-filling parameters [22], we derive an upper bound on the expected unregularized BIAN loss. Specifically, we utilize a probabilistic framework to analyze the learning dynamics of BIAN, establishing that as the number of training data points increases, the expected loss decreases with high probability. This bound offers a theoretical guarantee that, under certain regularity conditions, BIAN will converge to an accurate solution as the training set grows. Furthermore, we demonstrate that the convergence rate depends on the dimensionality of the problem and the smoothness of the underlying solution,

providing insight into the trade-offs between data complexity and model performance. These results lay the foundation for understanding the performance of BIAN in practical applications and offer a clear direction for optimizing its training process to enhance efficiency and accuracy.

3.1. The Mathematical Model

Taking consider with a PDE-constrained inverse problem with the form as,

$$\mathcal{L}(u(x), \varepsilon(x)) = f(x), \quad x \in \Omega \quad (3.1a)$$

$$u(x) = p(x), \quad x \in \Gamma_1 \quad (3.1b)$$

$$\frac{\partial u(x)}{\partial \mathbf{n}} = q(x), \quad x \in \Gamma_2 \quad (3.1c)$$

where $\mathcal{L}(\cdot)$ is the differential operator with the form as $\mathcal{L}(u(x), \varepsilon(x)) = -\nabla \cdot (\varepsilon(x) \nabla u(x))$, $\varepsilon(x)$ represents the indeterminate medium distribution. As BIAN is aim to deal with problems in which indeterminate parameters in the differential operator with a set of training data. The convergence rate of the first Neural Network, which serves as the approximator, plays a crucial role in determining the overall convergence speed of the algorithm. To solve this PDE-constrained inverse problem, we first rewrite the PDE as $-\nabla^2 u(x) = (f(x) + \nabla \varepsilon(x) \nabla u(x)) / \varepsilon(x)$ and the approximator is aim to approximate the evaluate source term. So that the loss function can be written as,

$$\mathbf{L}_a(x'_b; u_a) = \|R_a(x'_b; u_a)\|^2 = \|F(x'_b) - A[u_a](x'_b)\|^2 \quad (3.2)$$

where $F(x'_b) = m(x'_b) + \int_{\Gamma} n(x'_b) d\Gamma = c(x'_b)u(x'_b) + \int_{\Gamma} (u(x_b) \nabla G(x_b, x'_b) - G(x_b, x'_b) \nabla u(x_b)) \cdot d\Gamma(\mathbf{x}_b)$, $A[u_a](x'_b) = \int_{\Omega} z(x'_b; \theta_a) = \int_{\Omega} G(x_i, x'_b) u_a(x_i; \theta_a) d\Omega(x_i)$. We seek to find a neural network $u^* \in \mathcal{U}_n$ to minimize this loss function. The training data consist of one type of data sets: boundary source data. A boundary source datum is composed of the coordiante information and the two kinds of boundary conditions $(x'_b, u(x'_b), \partial u(x'_b) / \partial \mathbf{n})$, where $x'_b \in \partial U$. The set of m_b boundary source data is donated by $\mathcal{T}_b^{m_b} = \{\mathbf{x}'_{b_i}\}_{i=1}^{m_b}$.

Support $\mathcal{T}_b^{m_b}$ are samples obeying probability distributions μ_b . Since the empirical probability distribution on $\mathcal{T}_b^{m_b}$ defined by $\mu_b^{m_b} = \frac{1}{m_b} \sum_{i=1}^{m_b} \delta_{x'_{b_i}}$, the empirical loss function and expected loss function are obtained by taking the expectation on Equation (3.2) with respect to $\mu_b^{m_b}$ and μ_b , respectively.

$$\text{Loss}_m(u_a) = \mathbb{E}_{\mu_b^{m_b}}[\mathbf{L}_a(x'_b; u_a)] \quad (3.3a)$$

$$\text{Loss}(u_a) = \mathbb{E}_{\mu_b}[\mathbf{L}_a(x'_b; u_a)]. \quad (3.3b)$$

3.2. The Convergence Analysis

If the expected loss function were available, its minimizer would be the solution to Equation (4.1a) or close to it. However, it is unrealistic to get such function in practice, the empirical loss function is used as a substitute. We will give an upper bound of the expected loss function, which involves the empirical loss function. The derivation is

based on the probabilistic space filling arguments. In this regard, we make the following assumptions on the training data distributions.

Before the demonstration, we introduce the mathematical principle which helps the demonstration of the convergence theorem.

Definition 1 (Hölder Continuity). *Let $f : \mathbb{R}^n \rightarrow \mathbb{R}$ be a function, and let $\alpha \in (0, 1]$ and $C > 0$. We say that f is Hölder continuous with exponent α if for all $x, y \in \mathbb{R}^n$, the following inequality holds:*

$$|f(x) - f(y)| \leq C|x - y|^\alpha.$$

Here, α is called the Hölder exponent, and C is a Hölder constant. When $\alpha = 1$, the function f is said to be Lipschitz continuous.

We call $[f]_{\alpha;U}$, with the form of Equation (3.4), as the Hölder constant(coefficient) of f on U .

$$[f]_{\alpha;U} = \sup_{x,y \in U, x \neq y} \frac{|f(x) - f(y)|}{\|x - y\|^\alpha} < \infty, \quad 0 < \alpha \leq 1, \quad (3.4)$$

As the derivation is based on the probabilistic space filling arguments[23, 24]. In this regard, we make the following assumptions on the training data distributions.

Assumption 1. *Let U be a bounded domain in \mathbb{R}^d that is at least of class $C^{0,1}$ and Γ be a closed subset of ∂U . Let μ_b and μ_i be probability distributions defined on Γ and U , respectively. Let ρ_b be the probability density of μ_b with respect to $d - 1$ -dimensional Lebesgue measure on Γ . Let ρ_i be the probability density of μ_i with respect to d -dimensional Hausdorff measure on U .*

1. ρ_r and ρ_b are supported on \bar{U} and Γ , respectively. Also, $\inf_{\bar{U}} \rho_r > 0$ and $\inf_{\Gamma} \rho_b > 0$.
2. For $\varepsilon > 0$, there exists partitions of U and Γ , $\{U_j^\varepsilon\}_{j=1}^{K_r}$ and $\{\Gamma_j^\varepsilon\}_{j=1}^{K_b}$, that depend on ε , such that for each j , there are cubes $H_\varepsilon(z_{j,r})$ and $H_\varepsilon(z_{j,b})$ of side length ε centered at $z_{j,r} \in U_j^\varepsilon$ and $z_{j,b} \in \Gamma_j^\varepsilon$, respectively, satisfying $U_j^\varepsilon \subset H_\varepsilon(z_{j,r})$ and $\Gamma_j^\varepsilon \subset H_\varepsilon(z_{j,b})$.
3. For each m , \mathcal{H}_m contains a network u_m^* satisfying $Loss_m(h_m^*) = 0$.
4. There exist positive constants c_r, c_b such that $\forall \varepsilon > 0$, the partitions from the above satisfy $c_r \varepsilon^d \leq \mu_r(U_j^\varepsilon)$ and $c_b \varepsilon^{d-1} \leq \mu_b(\Gamma_j^\varepsilon)$ for all j .

There exist positive constants C_r, C_b such that $\forall x_r \in U$ and $\forall x_b \in \Gamma$, $\mu_r(B_\varepsilon(x_r) \cap U) \leq C_r \varepsilon^d$ and $\mu_b(B_\varepsilon(x_b) \cap \Gamma) \leq C_b \varepsilon^{d-1}$, where $B_\varepsilon(x)$ is a closed ball of radius ε centered at x .

Here C_r, c_r depend only on (U, μ_r) and C_b, c_b depend only on (Γ, μ_b) .

We remark that Assumption 1 guarantees that random samples drawn from probability distributions can fill up both the interior of the domain U and the boundary ∂U . These are mild assumptions and can be satisfied in many practical cases.

We now state our result that bounds the expected PINN loss in terms of the empirical loss. Let us recall that m is the vector of the number of training data points, i.e., $m = (m_b, m_i)$. The constants c_b, C_b, c_i, C_i are introduced in Assumption 3.1. For a function f , $[f]_{\alpha;U}$ is the Hölder constant of f with exponent α in U .

Theorem 1. *Suppose Assumption 3.1 holds. Let m_b and m_i be the number of i.i.d. samples from μ_b and μ_i , respectively. With probability at least, $(1 - \sqrt{m_b}(1 - 1/\sqrt{m_b})^{m_b})$, we have*

$$\text{Loss}(u_a) \leq C'_1 \text{Loss}_m(u_a) + C'_{max} (m_b^{-\frac{a}{d-1}-0.5} + m_b^{-\frac{2a+d}{2(d-1)}}), \quad (3.5)$$

here $C'_1 = 3\frac{C_b}{c_b} m_b^{0.5} \sqrt{d}^{2d-1}$ and $C'_{max} = \max\{2[n]_{a,U}^2 d^{\frac{2a+d-1}{2}} c_b^{-\frac{2a}{d-1}-1}, 2[z]_{a,U}^2 d^{\frac{2a+d}{2}} c_b^{\frac{2a+d}{d-1}}\}$.

Proof. The proof can be found in Appendix A. \square

The number of training data is depends on the number of boundary point. We can obtain

$$\text{Loss}(u_a) = O(m_b^{-\frac{a}{d-1}-0.5}). \quad (3.6)$$

From Theorem 1, we establish the relationship between the convergence rate of BIAN with the number of boundary data number. In the next section, we provide a numerical experiment to illustrate our theoretical findings. Also, experiments to prove the feasibility and accuracy of BIAN have been conducted.

4. Numerical Examples

In order to demonstrate the accuracy and convergence of BIAN in solving PDE-constrained inverse problem, a series of numerical experiments were conducted to analyze its performance advantages over existing methods, such as PINN, WAN and DRM, in scenarios involving spatially varying and piecewise uniform indeterminate medium distributions. Furthermore, we evaluate the stability and robustness of the multi-neural network co-optimization algorithm during training.

The results of these experiments provide comprehensive insights into the superioring of BIAN in addressing complex inverse problems, showcasing its potential for practical applications in various fields such as engineering and physics. The following sections presents a detailed description of the numerical experimental setup, methodologies, and findings, exphasizing the advantages of the proposed approach over traditional techniques.

4.1. Evaluation of Computational Feasibility

Numerical experiments were conducted for the two-dimensional Laplace problem, with the objective of comparing with traditional methods, including Physics-Informed Neural Networks (PINN), Deep Ritz Method (DRM), and Weak Adversarial Networks (WAN). The key metrics evaluated included computational time, resource usage, and scalability.

Consider the Laplace equation with spatially varying indeterminate medium distribution:

$$-\nabla \cdot (\varepsilon(\mathbf{x}) \nabla u(\mathbf{x})) = 0, \quad \mathbf{x} \in \Omega \quad (4.1a)$$

$$u(\mathbf{x}) = \sin(\pi y), \quad \mathbf{x} \in \Gamma_1 \quad (4.1b)$$

$$u(\mathbf{x}) = 0, \quad \mathbf{x} \in \Gamma_2 \quad (4.1c)$$

Here $\Omega \in [0, 1]^2$, $\Gamma_1 = \{(x, y) | x \in \{0, 1\}, y \in [0, 1]\}$, $\Gamma_2 = \partial\Omega \setminus \Gamma_1$, $\varepsilon(\mathbf{x}) = e^{\pi^2(x-x^2)/2}/\pi$, the solution of this problem $u(\mathbf{x}) = e^{\pi^2(x^2-x)/2} \cdot \sin(\pi y)$. The natural boundary condition can be obtained from the analytical expression of the solution. The solution and the medium distribution of the Laplace problem is shown as Figure 4.1.

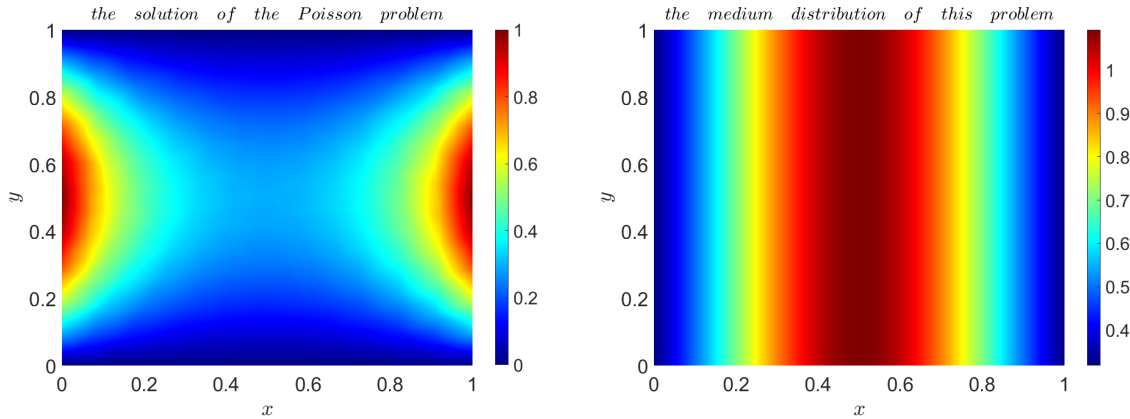


Figure 3. The solution and the medium distribution of the Laplace problem.

Each layer of the residual blocks in the approximator and generator we used to solve this problem has $m = 10$ neurons, and there are a total of 400 parameters in this model. We select 10 points on each boundary as the boundary source points $\{x_b\}$ and 100 random points inside the domain as the internal source point $\{x_i\}$. Since we want to compare this method with existing methods, such as PINN, DRM and WAN, the three methods are also utilized to solve this Laplace problem. For the three methods, we use a multilayer perceptron (MLP) with 4 hidden layers and each layer has 10 neurons and we choose 500 random points as the training points.

The solution and the medium distribution obtained from each method is shown as follows and the L_2 error of each method is shown in Table 1. By comparing the results from different methods, it is evident that BIAN not only demonstrates better accuracy but also achieves faster convergence compared to the other three proposed methods. More importantly, BIAN requires only boundary information to solve the problem, significantly simplifying the data acquisition process.

Table 1. The L_2 error of the solution and medium distribution for the four methods

Method	PINN	WAN	DRM	BIAN
L_2 error				
medium distribution	0.0313	0.0526	0.9872	0.0143
solution	0.3117	0.2978	0.2281	0.0121

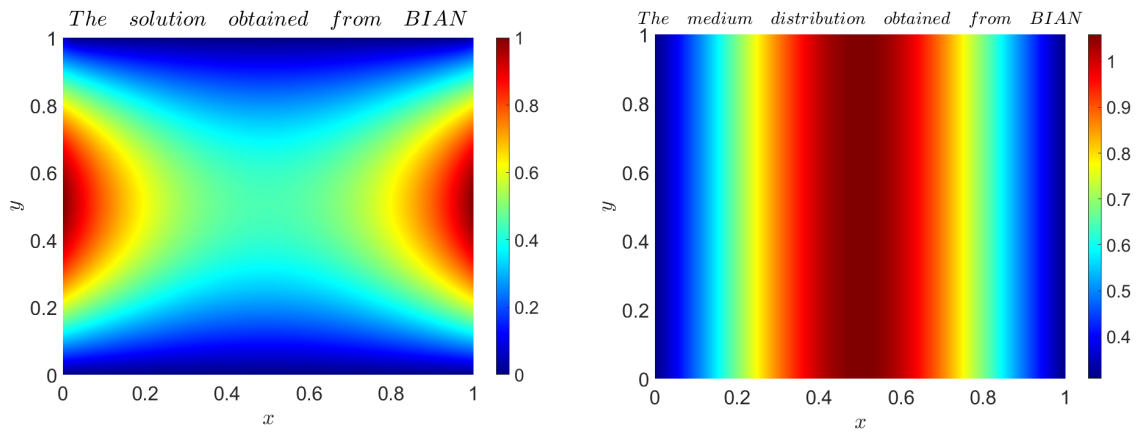


Figure 4. The solution and the medium distribution of the Laplace problem obtained from BIAN.

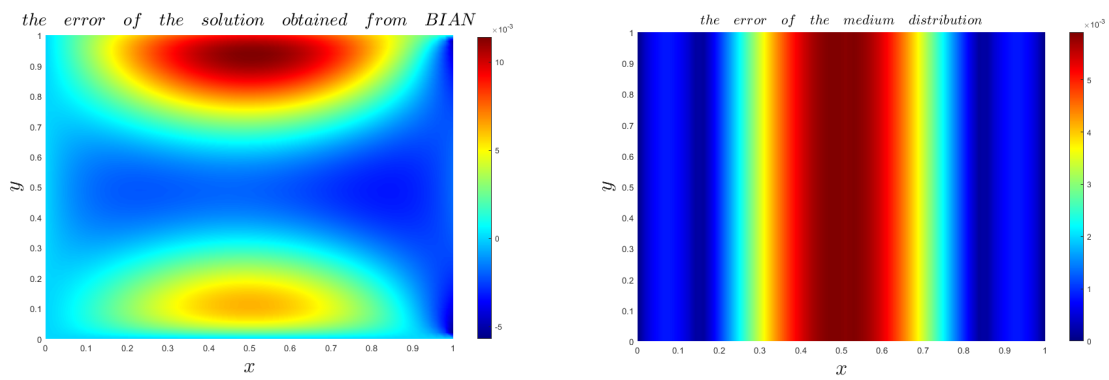


Figure 5. The solution and the medium distribution of the Laplace problem obtained from BIAN.

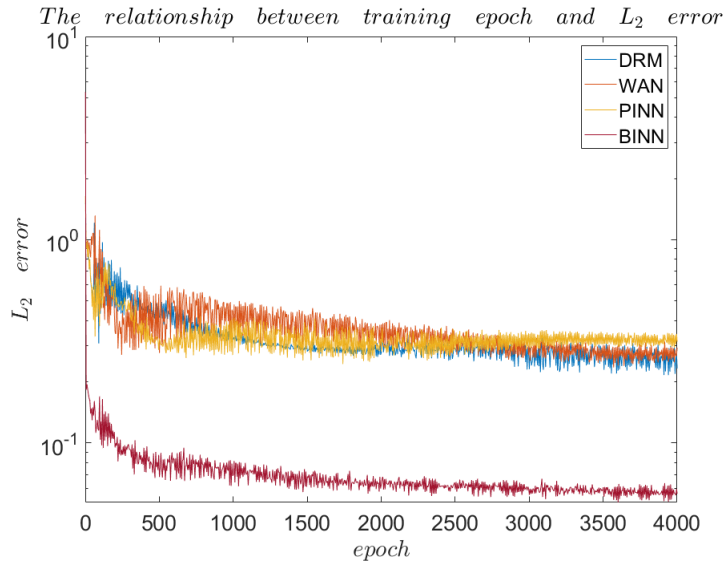


Figure 6. The relationship between the training epoch and the L_2 error of the solution.

From Figure 4 and Figure 5, we can find that the approximation error of the medium distribution occurs not only in the middle part of the solution domain but also near the boundaries. The error in the middle part mainly because the lack of known medium distribution and the error near the boundaries may be caused by the singular integral when training the neural network. Figure 6 shows that BIAN has a better solution accuracy than the other three methods with the same training epoch.

4.2. The convergence analysis

In this experiment, we aim to compare the advantages of BIAN over traditional methods in terms of convergence speed. Specifically, we focus on evaluating how BIAN performs in scenarios with varying medium distributions. We will analyze the convergence rates for BIAN and benchmark them against traditional approaches to highlight the efficiency gains that BIAN provides in solving complex inverse problems. Through this comparison, we aim to demonstrate the superior convergence performance of BIAN in handling high-dimensional and non-linear cases, where traditional methods may struggle to achieve the same level of accuracy and computational efficiency.

The problem to be solved in this experiment, as well as the architecture of the neural network, are identical to those used in Section 4.1. We focus on comparing the relationship between solution accuracy and the size of the training data for BIAN and PINN when applied to the same problem. Specifically, we aim to assess how the two methods scale in terms of accuracy as the amount of training data increases. By examining this relationship, we can gain insights into the data efficiency of BIAN compared to PINN, particularly in high-dimensional and complex scenarios. This comparison is crucial for understanding the trade-offs between data size and solution precision, and it highlights the potential advantages of BIAN in reducing the need for extensive training data while maintaining or improving accuracy. Figure 11 shows the relationship between the number of training data and the L_2 error. As a reference,

The $O(m^{-1.5})$ rata of convergence is plotted as a dotted line. As we can see, with the same number of training data, BIAN achieves higher accuracy compared with IPINN. Additionally, BIAN exhibits faster convergence rate compared with IPINN.

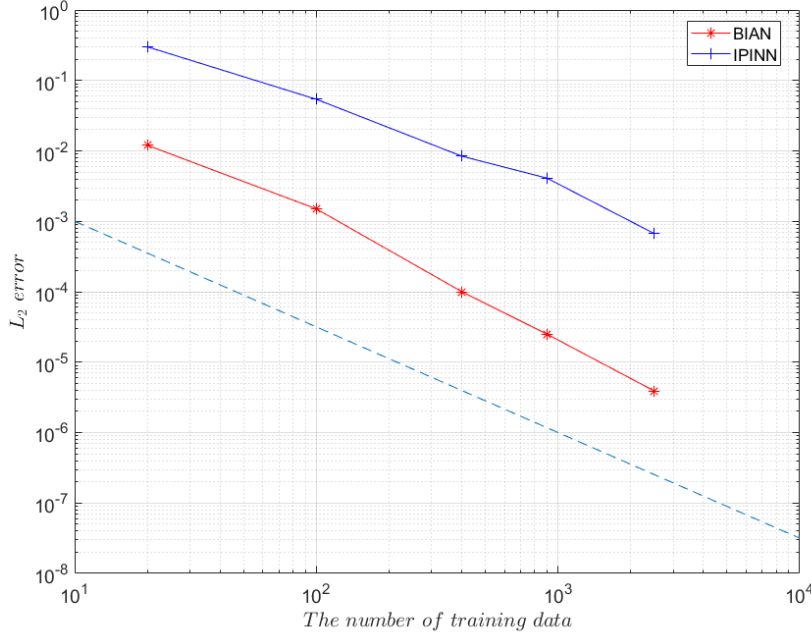


Figure 7. The relationship between the number of training data and the L_2 error of the solution.

4.3. Dealing with Piecewise uniform medium distribution

The following experiment is designed to demonstrate the effectiveness of BIAN in solving problems with piecewise uniform medium distributions. The results will highlight the performance of BIAN in terms of computational accuracy and efficiency, further establishing its potential as a robust method for solving complex inverse problems.

Consider the Poisson equation with indeterminate piecewise uniform medium distribution:

$$-\nabla \cdot (\varepsilon(\mathbf{x})\nabla u(\mathbf{x})) = f(\mathbf{x}), \quad \mathbf{x} \in \Omega \quad (4.2a)$$

$$u(\mathbf{x}) = 1, \quad \mathbf{x} \in \Gamma_1 \quad (4.2b)$$

$$u(\mathbf{x}) = 0, \quad \mathbf{x} \in \Gamma_2 \quad (4.2c)$$

Here $\Omega = \{(x, y) | (x, y) \in (0, 1) \times (0, 1) / (0.5) \times (0.5, 1)\}$, $\Gamma_1 = \{(x, y) | x \in \{0\}, y \in [0, 1]\}$, $\Gamma_2 = \partial\Omega \setminus \Gamma_1$, $\varepsilon(\mathbf{x}) = 10$ when $\mathbf{x} = \{(x, y) | (x, y) = (0, 1) \times (0, 0.5)\}$, $\varepsilon(\mathbf{x}) = 5$ when $\mathbf{x} = \{(x, y) | (x, y) = (0.5, 1) \times (0.5, 1)\}$ and $f(x) = 1$. However, the two kinds of boundary conditions are all needed when utilizing BIAN to solve the inverse problems, we obtain the natural boundary condition for this problem with the Finite difference Method (FDM). The solution and the medium distribution of the Laplace problem is shown as Figure 4.1, and we can get the analytical solution of the natural boundary condition. Each layer of the residual blocks in the approximator network and generator network we used to solve this problem has $m = 10$ nerurons, there are a total of 400

parameters in this model. We select 10 evenly spaced points on each boundary as the boundary source points $\{x_b\}$ and 100 random points inside the domain as the internal source point $\{x_i\}$.

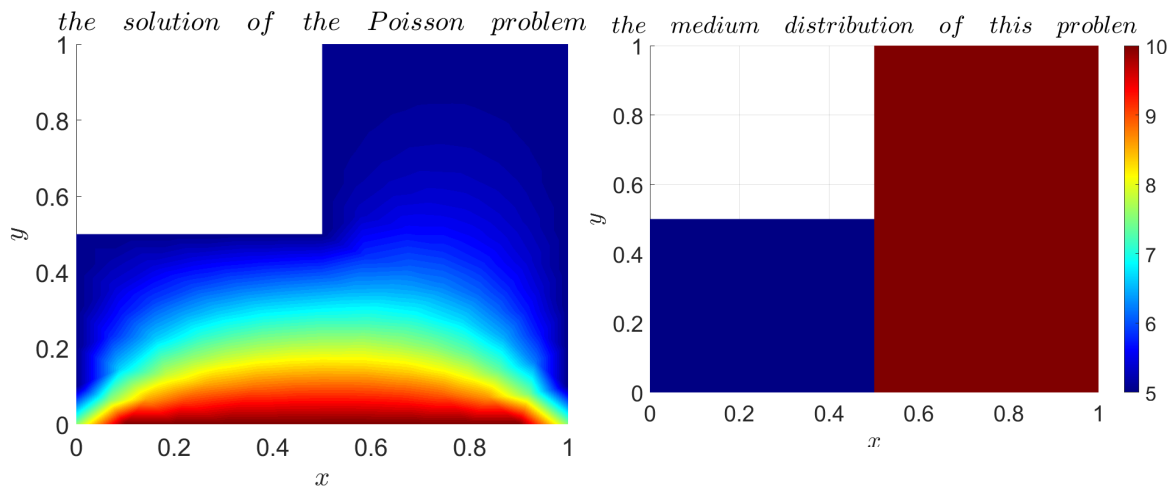


Figure 8. The solution and the medium distribution of the Poisson problem.

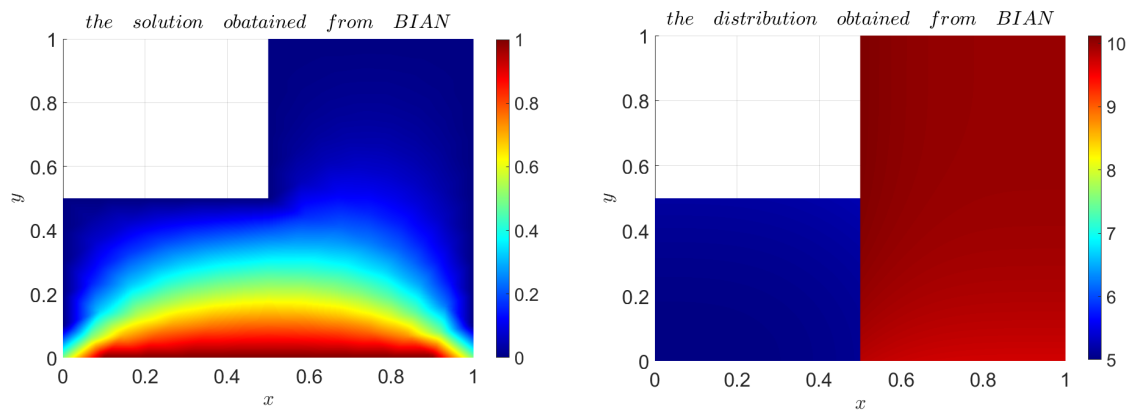


Figure 9. The solution and the medium distribution of the Poisson problem obtained from BIAN.

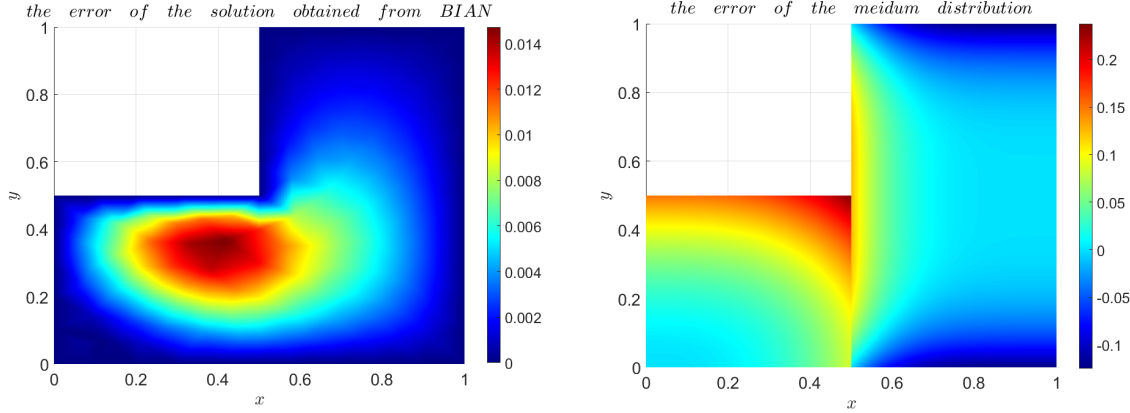


Figure 10. The error of the solution and the medium distribution of the Poisson problem.

The solution and the medium distribution approximated by BIAN is shown as Figure 10. The L_2 errors of the solution and medium distribution are 0.0079 and 0.069, respectively. From this numerical experiment, it proves that BIAN can not only deal with spatially varying medium distribution problems but also solve the piecewise uniform medium distribution problems.

4.4. Dealing with High-dimensional problems

Consider a 3-D problem with unknown medium distribution, whose form is shown as follows:

$$-\nabla \cdot (\varepsilon(\mathbf{x})\nabla u(\mathbf{x})) = f(\mathbf{x}), \quad x \in [0, 1]^3 \quad (4.3a)$$

$$u|_{\partial[0,1]^3} = 0, \quad x \in \partial[0, 1]^3. \quad (4.3b)$$

$$(4.3c)$$

where the source term $f(x) = 1$ and the unknown medium distribution $\varepsilon(\mathbf{x}) = \sum_k x_k$. Such problem can be easily solved through numerical method while the medium distribution has already known. However, it is notoriously difficult to reconstruct the unknown medium distribution due to the curse of dimensionality, which often leads to slow convergence, significant computational complexity.

The approximator network and generator network we used to solve this problem has $m = 10$ nerurons, there are a total of 400 parameters in this model. We select 100 evenly spaced points on each boundary as the boundary source points $\{x_b\}$ and 1000 random points inside the domain as the internal source point $\{x_i\}$.

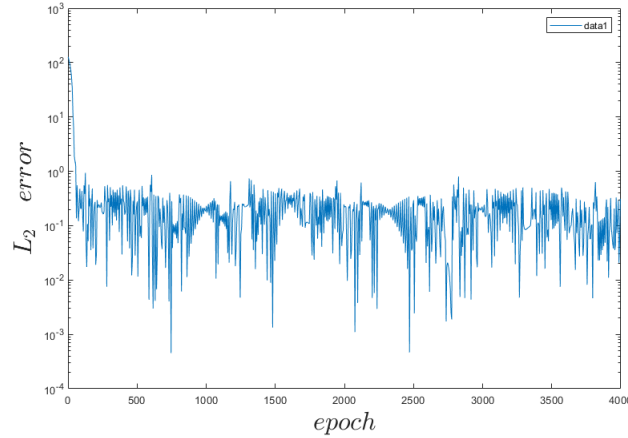


Figure 11. The relationship between the training epoch and the L_2 error of the solution.

From Figure 11, it can be observed that with the dimensionality increasing, the solving speed of BIAN does not reduce. Compared to the two-dimensional problem, BIAN can still achieve a relatively accurate result within 500 training iterations for the three-dimensional problem. However, the solution accuracy shows a certain decrease compared to the two-dimensional case, which because the convergence rate of BIAN is affected by the dimensionality, and with the same amount of data, the training performance of BIAN gradually decreases as the dimensionality increases. What's more, the oscillation of L_2 error during the training epoch may be caused by the random source points within the domain.

5. Conclusion

In this work, we proposed a novel method based on representing medium coefficients with a neural network to solve inverse problems. This method, Boundary-Informed Alone Neural Network (BIAN), offers several significant advantages:

- With the incorporation of Green's theorem of energy conservation, the relationship between boundary energy flux and the energy distribution within the solution domain has been established. There is no need for inner points when training the neural network, which provides significant assistance in addressing practical issues. Moreover, measurement points can be sampled relatively uniformly along the boundary, mitigating the issue of non-uniform sample data distribution.
- The method exhibits strong performance in approximating complex functions and solving high-dimensional problems due to the high-dimensional capabilities of neural networks.
- With the collaborative training between three neural networks, both training accuracy and convergence speed are enhanced compared to when the two neural networks are trained independently.

- This method is capable of achieving higher accuracy under the same training data. Moreover, it demonstrates a faster convergence rate, making it more efficient in solving complex problems. The combination of improved precision and quicker convergence not only reduces computational time but also enhances the overall performance, particularly in scenarios where data availability is limited or problem complexity increases.

However, we also some disadvantages that could be addressed in future works.

- The integral term in the loss function requires computation via Gaussian integration, which may lead to a reduction in solution accuracy.
- When dealing with piecewise medium problems, the position of the interface between the two media is essential. Inferring the position of medium distribution from data may be impractical

Future research could explore the introduction of new neural network architectures, novel optimization algorithms, and advanced activation functions to potentially yield superior results. The numerical experiments conducted demonstrate BIAN's superior computational accuracy and efficiency compared to existing methods such as PINN, DRM, and WAN, particularly in solving problems with piecewise uniform medium distributions. This work highlights the potential of BIAN as a robust method for solving complex inverse problems, paving the way for its application in various fields such as engineering and physical sciences.

Appendix A. Proof of Theorem 1

The proof consists two lemmas.

Lemma 1. *Let $\mathcal{T}_b^{m_b} = \{\mathbf{x}'_{b_i}\}_{i=1}^{m_b}$. Support m_b is large enough to satisfy the following: for any $x'_b \in \Gamma$, there exists $x''_b \in \mathcal{T}_b$ such that $\|x'_b - x''_b\| \leq \epsilon_r$. Then we can get:*

$$\text{Loss}(u_a) \leq C_1 \text{Loss}_m(u_a) + C_{max}(\epsilon_b^{2a} + \epsilon_b^{2a+d-1} + \epsilon_i^{2a+d}) \quad (\text{A.1})$$

where $C_1 = 3C_b C_i m_b m_i \epsilon_b^{d-1} \epsilon_i^d$ and $C_{max} = \max\{2[m]_{a,U}^2, 2[n]_{a,U}^2, 2[z]_{a,U}^2\}$.

Proof. Let first consider the extended form of Cauchy-Schwarz inequality $\|x + y + z\|^2 \leq 3(\|x\|^2 + \|y\|^2 + \|z\|^2)$. For $x'_b, x'_i \in U$, we have

$$\begin{aligned} \mathbf{L}_a(x'_b; u_a) &= \|F(x'_b) - A[u_a](x'_b)\|^2 \\ &= \|F(x'_b) - F(x''_b) + F(x''_b) - A[u_a](x''_b) + A[u_a](x''_b) - A[u_a](x'_b)\|^2 \\ &\leq 3(\|F(x'_b) - F(x''_b)\|^2 + \|F(x''_b) - A[u_a](x''_b)\|^2 \\ &\quad + \|A[u_a](x''_b) - A[u_a](x'_b)\|^2) \end{aligned} \quad (\text{A.2})$$

By assumption, $\forall x'_b \in \Gamma$, there exists $x''_b \in \mathcal{T}_b^{m_b}$ satisfied $\|x'_b - x''_b\| \leq \epsilon_b$. Then we can get

$$\|F(x'_b, x_b) - F(x''_b, x_b)\|^2 = \|m(x'_b) - m(x''_b) + \int_{\Gamma} n(x'_b) d\Gamma - \int_{\Gamma} n(x''_b) d\Gamma\|^2$$

$$\begin{aligned}
&\leq 2\|m(x'_b) - m(x''_b)\|^2 + 2 \int_{\Gamma} \|n(x'_b) - n(x''_b)\|^2 d\Gamma \\
&\leq 2\epsilon_b^{d-1} \epsilon_b^{2a} [n]_{a,U}^2
\end{aligned} \tag{A.3}$$

$$\begin{aligned}
\|A[u_a](x''_b) - A[u_a](x'_b)\|^2 &= \left\| \int_{\Omega} z(x''_b; \theta_a) d\Omega - \int_{\Omega} z(x'_b; \theta_a) d\Omega \right\|^2 \\
&\leq \int_{\Omega} \|z(x''_b; \theta_a) - z(x'_b; \theta_a)\|^2 d\Omega \\
&\leq \epsilon_d^d \epsilon_d^{2a} [z]_{a,U}^2
\end{aligned} \tag{A.4}$$

$$L(x_b, x_i; h) \leq 3L(x'_b, x'_i; h) + 2\epsilon_b^{2a+d-1} [n]_{a,U}^2 + \epsilon_d^{2a+d} [z]_{a,U}^2 \tag{A.5}$$

For $x'_{b_i} \in \mathcal{T}_b^{m_b}$, $A_{x'_{b_i}}$ is the Voroni cell associated with x'_{b_i} , i.e.

$$A_{x'_{b_i}} = \left\{ \mathbf{x} \in U \mid \|\mathbf{x} - x'_{b_i}\| = \min_{\mathbf{x}' \in \mathcal{T}_b^{m_b}} \|\mathbf{x} - \mathbf{x}'\| \right\},$$

Let $\gamma_b^i = \mu_b(A_{x'_{b_i}})$ which satisfies $\sum_{i=1}^{m_b} \gamma_b^i = 1$. Taking the expectation with respect to $(x_b) \sim \mu_b$, we have

$$\begin{aligned}
\text{Loss}(h) &\leq 3 \sum_{i=1}^{m_b} \gamma_b^i \mathbf{L}_a(x'_b; u_a) \\
&\quad + 2\epsilon_b^{2a+d-1} [n]_{a,U}^2 + \epsilon_d^{2a+d} [z]_{a,U}^2
\end{aligned} \tag{A.6}$$

With $\gamma_b^{m_b,*} = \max_i \gamma_b^i$, we can obtain

$$\begin{aligned}
\text{Loss}(h) &\leq 3m_b \gamma_b^{m_b,*} \frac{1}{m_b} \sum_{i=1}^{m_b} \gamma_b^i \mathbf{L}_a(x'_b; u_a) \\
&\quad + 2\epsilon_b^{2a+d-1} [n]_{a,U}^2 + \epsilon_d^{2a+d} [z]_{a,U}^2
\end{aligned} \tag{A.7}$$

Note that $m_b \gamma_b^{m_b,*} \geq 1$. Let $B_{\epsilon}(\mathbf{x})$ be a closed ball centered at \mathbf{x} with radius ϵ . Let $P_b^* = \max_{\mathbf{x} \in \Gamma} \mu_b(B_{\epsilon_b}(\mathbf{x}) \cap \Gamma)$. Since for any $\mathbf{x}_b \in \Gamma$, there exists $\mathbf{x}'_b \in \mathcal{T}_b^{m_b}$ such that $\|\mathbf{x}'_b - \mathbf{x}_b\| \leq \epsilon_b$ for each i , there are closed balls B_{ϵ_b} that include $A_{\mathbf{x}'_b}$. Thus, we have $\gamma_b^{m_b,*} \leq P_b^*$. Moreover, it follows from Assumption 1 that

$$\gamma_b^{m_b,*} \leq P_b^* \leq C_b \epsilon_b^{d-1}. \tag{A.8}$$

Therefore we can get

$$\text{Loss}(h) \leq C_1 \text{Loss}_m(h) + C_{max} (\epsilon_b^{2a+d-1} + \epsilon_d^{2a+d}) \tag{A.9}$$

where $C_1 = 3C_b m_b \epsilon_b^{2d-1}$ and $C_{max} = \max\{2[n]_{a,U}^2, 2[z]_{a,U}^2\}$. The proof is completed. \square

Lemma 2. *Let X be a compact subset in \mathbb{R}^d . Let μ be a probability measure supported on X . Let ρ be the probability density of μ with respect to s -dimensional Hausdorff measure on X such that $\inf_{X_{\rho}} > 0$. Suppose that for $\epsilon > 0$, there exists a partition of X , $\{X_k^{\epsilon}\}_{k=1}^{K_{\epsilon}}$ that depends on ϵ such that for each X_k^{ϵ} , $c\epsilon^s \leq \mu(X_k^{\epsilon})$ where $c > 0$ depends only on (μ, X) , and there exists a cube $H_{\epsilon}(z_k)$ of side length ϵ centered at some z_k in X_k^{ϵ} such that $X_k^{\epsilon} \subset H_{\epsilon}(z_k)$. Then, with probability at least $1 - \sqrt{n}(1 - 1/\sqrt{n})^n$ over*

iid n sample points $\{x_i\}_{i=1}^n$ from μ , for any $x \in X$, there exists a point x_j such that $\|x - x_j\| \leq \sqrt{dc}^{-\frac{1}{s}} n^{-\frac{1}{2s}}$.

Proof. The proof of this lemma has already been proven in Appendix B of [18]. \square

By lemma 2, with the probability at least

$$(1 - \sqrt{m_b}(1 - 1/\sqrt{m_b})^{m_b}), \quad (\text{A.10})$$

$\forall x_b \in \Gamma$, there exists $\mathbf{x}'_b \in \mathcal{T}_b^{m_b}$ satisfied $\|\mathbf{x}'_b - \mathbf{x}''_b\| \leq \sqrt{dc}^{-\frac{1}{d-1}} m_b^{-\frac{1}{2(d-1)}}$. By letting $\epsilon_b = \sqrt{dc}^{-\frac{1}{d-1}} m_b^{-\frac{1}{2(d-1)}}$, with the probability at least Equation (A.10), we have

$$\text{Loss}(u_a) \leq C'_1 \text{Loss}_m(u_a) + C'_{max} (m_b^{-\frac{a}{d-1}-0.5} + m_b^{-\frac{2a+d}{2(d-1)}}) \quad (\text{A.11})$$

where $C'_1 = 3\frac{C_b}{c_b} m_b^{0.5} \sqrt{d}^{2d-1}$ and $C_{max} = \max\{2[n]_{a,U}^2 d^{\frac{2a+d-1}{2}} c_b^{-\frac{2a}{d-1}-1}, 2[z]_{a,U}^2 d^{\frac{2a+d}{2}} c_b^{\frac{2a+d}{d-1}}\}$. The proof is completed.

References

- [1] Richard C. Aster, Clifford H. Thurber, and Brian Borchers. *Parameter Estimation and Inverse Problems*. Number v. 90 in International Geophysics Series. Elsevier Academic Press.
- [2] Simon Arridge, Peter Maass, Ozan Öktem, and Carola-Bibiane Schönlieb. Solving inverse problems using data-driven models. 28:1–174.
- [3] Jonas Adler and Ozan Öktem. Solving ill-posed inverse problems using iterative deep neural networks. *Inverse Problems*, 33(12):124007, nov 2017.
- [4] Markus Reichstein, Gustau Camps-Valls, Bjorn Stevens, Martin Jung, Joachim Denzler, Nuno Carvalhais, and Prabhat. Deep learning and process understanding for data-driven Earth system science. 566(7743):195–204.
- [5] Yasushi Ota, Yu Jiang, and Daiki Maki. Parameters identification for an inverse problem arising from a binary option using a bayesian inference approach. *Results in Applied Mathematics*, 17:100353, 2023.
- [6] Lawrence C Evans. *Partial differential equations*, volume 19. American Mathematical Society, 2022.
- [7] Derick Nganyu Tanyu, Jianfeng Ning, Tom Freudenberg, Nick Heilenkötter, Andreas Rademacher, Uwe Iben, and Peter Maass. Deep learning methods for partial differential equations and related parameter identification problems. *Inverse Problems*, 39(10):103001, aug 2023.
- [8] M. Raissi, P. Perdikaris, and G.E. Karniadakis. Physics-informed neural networks: A deep learning framework for solving forward and inverse problems involving nonlinear partial differential equations. 378:686–707.
- [9] Weinan E and Bing Yu. The Deep Ritz Method: A Deep Learning-Based Numerical Algorithm for Solving Variational Problems. 6(1):1–12.
- [10] Yaohua Zang, Gang Bao, Xiaojing Ye, and Haomin Zhou. Weak adversarial networks for high-dimensional partial differential equations. *Journal of Computational Physics*, 411:109409, 2020.
- [11] Paul Davis and Şerban Raianu. Computing areas using Green’s Theorem and a Software Planimeter. *Teaching Mathematics and its Applications: An International Journal of the IMA*, 26(2):103–108, 06 2007.
- [12] Andreas Kirsch. *An Introduction to the Mathematical Theory of Inverse Problems*, volume 120 of *Applied Mathematical Sciences*. Springer International Publishing.
- [13] Ian J. Goodfellow, Jean Pouget-Abadie, Mehdi Mirza, Bing Xu, David Warde-Farley, Sherjil Ozair, Aaron Courville, and Yoshua Bengio. Generative adversarial networks, 2014.

- [14] Prajit Ramachandran, Barret Zoph, and Quoc Le. Swish: a self-gated activation function. 10 2017.
- [15] Hao-Jie Hu, Jiawen Li, Li-Ye Xiao, Yu Cheng, and Qing Huo Liu. A residual fully convolutional network (res-fcn) for electromagnetic inversion of high contrast scatterers at an arbitrary frequency within a wide frequency band. *Inverse Problems*, 40(6):065008, may 2024.
- [16] Carsten Carstensen, Stefan Funken, and Ernst Stephan. A posteriori error estimates for boundary element methods. *Applicable Analysis*, 61:233–253, 08 1996.
- [17] Flemming Topsøe and Bent Fuglede. Jensen-shannon divergence and hilbert space embedding. *IEEE*, 2005.
- [18] Yeonjong Shin, Jérôme Darbon, and George Em Karniadakis. On the convergence of physics informed neural networks for linear second-order elliptic and parabolic type pdes. *Communications in Computational Physics*, 2020.
- [19] Tao Luo and Haizhao Yang. Two-layer neural networks for partial differential equations: Optimization and generalization theory, 2020.
- [20] Qingguo Hong, Jonathan W. Siegel, and Jinchao Xu. A priori analysis of stable neural network solutions to numerical pdes, 2022.
- [21] Zhiqiang Cai, Jingshuang Chen, Min Liu, and Xinyu Liu. Deep least-squares methods: An unsupervised learning-based numerical method for solving elliptic pdes. *Journal of Computational Physics*, 420:109707, 2020.
- [22] Xin-dang He, Wen-xuan Gou, Yong-shou Liu, and Zong-zhan Gao. A practical method of nonprobabilistic reliability and parameter sensitivity analysis based on space-filling design. *Mathematical Problems in Engineering*, 2015(1):561202, 2015.
- [23] Jeff Calder. Consistency of lipschitz learning with infinite unlabeled data and finite labeled data. *SIAM Journal on Mathematics of Data Science*, 1(4):780–812, 2019.
- [24] Chris Finlay, Jeff Calder, Bilal Abbasi, and Adam Oberman. Lipschitz regularized deep neural networks generalize and are adversarially robust, 2019.